PHYSICSAccess Research Paper
ISSN Online: 2756-3898, ISSN Print: 2714-500X https://doi.org/10.47514/phyaccess.2023.3.1.007

First-principles Study on the Structural, Electronic, and Elastic Properties of Transition Metal Dichalcogenides

Shehu A Yamusa[1, 2], Amiruddin Shaari[2], Ibrahim Isah[3], Basima Farzan[4], Magaji Ismail[5], Summanuwa T Ahams[6] and Yahaya S Itas[7]

[1] Department of Physics, Faculty of Science, Federal College of Education, Zaria, Kaduna State, Nigeria
[2] Department of Physics, Faculty of Science, Universiti Teknologi, Malaysia
[3] Department of Science Laboratory Technology, Jigawa State Polytechnic, Dutse, Jigawa State, Nigeria
[4] Department of Physics, Faryab University, Afghanistan
[5] Department of Physics, Faculty of Science, Kaduna State University, Kaduna, Kaduna State, Nigeria
[6] Department of Physics, Faculty of Science, Adamawa State University, Mubi, Adamawa State, Nigeria
[7] Department of Physics, Bauchi State University, Gadau, Bauchi State, Nigeria

Corresponding E-mail: shehu@graduate.utm.my

Received 22-03-2023
Accepted for publication 19-04-2023
Published 20-04-2024

Abstract

In this paper, the structural, electronic, and elastic properties of molybdenum disulfide (MoS_2) in hexagonal and trigonal phases were investigated using first-principles calculations based on density functional theory (DFT) as implemented in the Quantum ESPRESSO package. Our findings from the structural and electronic properties of MoS_2 show that bulk hexagonal and trigonal MoS_2 phases have a calculated bandgap of 1.37 and 1.56 eV respectively, which is in good agreement with available theoretical and experimental results. The elastic properties show that both space groups of MoS_2 are brittle at zero pressure and they also agree with Born's mechanical stability condition. The overall results place our new optimized MoS_2 as a potential candidate for optoelectronic application.

Keywords: DFT; Transition metal dichalcogenides; anisotropy; chalcogen; elastic constants.

I. INTRODUCTION

Transition metal dichalcogenides (TMDs) have piqued research interests globally due to their promising applications in the area of optoelectronics [1], spintronics [2], and nanoelectronics [3]. MoS_2 has been identified as one of the momentous 2D materials for the study of semiconductors and their application in physics and engineering [4], since its discovery. Graphene was the first thoroughly investigated 2D material [5], which offers distinct advantages because of its high electron mobility and thermal conductivity which made it suitable for electronic and mechanical strength applications [6]. Graphene is a hexagonal carbon sheet with a two-dimensional structure and is immensely popular, but its zero bandgaps have sparked a search for 2D materials with semiconducting capabilities and applications [7-9].

TMDs are semiconductors materials of the general form MX_2 (M = Mo, W, etc.; X = S, Se, or Te) [10], the M is metal bonded to the non-metal called cuhalcogen X. Recently, revitalized interests of scientists and engineers in studying their structural, electrical, and elastic properties boosted to investigate its potential candidacy for the next generations of sustainability science and technology. TMDs exist in different phases with distinct space group numbers, with a lot of novels

that can also be used for many applications. Recent studies have been conducted on different phases of these materials and are found to be promising candidates for optoelectronic properties. For example, [11] studied the structural, electronic, and optical properties of WS2. Two bulk phases of WS2 with hexagonal phases and space group (P63/mmc) and rhombohedral phase (R3m) have been investigated and reported to be structurally stable both thermodynamically and dynamically. Reference [12] also investigated the electronic and optical properties of the hexagonal structure of the MoS_2 crystal for bulk and monolayer of MoS_2. A subsequent study by [13] used a self-consistent plane-wave method based on the DFT technique as implemented in the Quantum ESPRESSO using GGA-PW91, and their result demonstrates that the calculated lattice parameters overestimate the experimental values, which is a fundamental characteristic of standard GGA functional differing from experimental values [14, 15]. Reference [16] presented a study on the electronic, structural, and optical properties of graphene-like MoX2 using FP-LAPW + lo method in the WIEN2K simulation code. Similarly, [17] investigated the elastic properties of molybdenum disulfide using first-principles calculations, the authors calculated the elastic constant C_{ij} of MoS_2 at a pressure ranging from 0 to 40 GPa, while [18] presented a study on the electronic and elastic properties of hexagonal layered crystals using van der Waals functional, with results indicating a monotonical increase in the elastic constant of MoS_2 and an increase in the anisotropies of MoS_2 with an increase in pressure.

Research on MoS_2 has focused on the hexagonal space group's electronic, structural, and elastic capabilities, with little attention paid to the trigonal space group. However, earlier research has revealed that MoS_2 exists in different phases [19], with the graphene-like hexagonal bulk MoS_2 being given more attention [20]. Furthermore, to the best of our knowledge, there is no comprehensive study of the structural, electronic, and elastic properties of a trigonal phase of bulk MoS_2. As a result, research into the electrical and elastic characteristics is required.

The present work is arranged as follows: An overview of the extensive computational framework used in this work is provided in Section 2. In Section 3, the results are illustrated together with physical explanations of the elastic, structural, and electrical characteristics of the materials under study. In Section 4, final remarks were made.

II. Computational Framework

In this work, the Materials Project (MP) database served as the primary source of the crystal structures [21]. A density functional theory (DFT) [22] based calculations have been applied using the generalized gradient approximation (GGA) [23] as implemented in the Quantum ESPRESSO package [24, 25] employing the Perdew-Burke-Ernzerhof (PBE) variant for the exchange and correlation potentials. To improve the computation efficiency, the crystal structures of the two space groups were fully relaxed at zero pressure until the forces on each atom were less than 0.01 eV/Å, in which the optimized coordinates of MoS_2 have been used for the calculations. A $12 \times 12 \times 3$ Monk Horst-Pack [26] of k-points was used for the sampling in the Brillouin zone. The spacing of the real space grid used to calculate the Hartree, exchange, and correlation contribution to the total energy and Hamiltonian was 400 Ry. A supplementary package to the quantum ESPRESSO thermo_pw [27] was also used in the calculation of the elastic properties using an energy cut-off of 60 Ry in conjunction with $12 \times 12 \times 3$ for both hexagonal and the trigonal space group.

III. Results and Discussions

A. Equilibrium Lattice Parameters

Molybdenum disulfide has a hexagonal $P63/mmc$ $[no194]$ with lattice parameters $a = 3.19$ Å and $c = 13.98$ Å and trigonal $P\bar{3}m1$ $[no164]$ with a lattice parameter of $a = 3.19$Å and $c = 24.88$ Å. The structural model of MoS_2 comprises Mo and S layers as shown in Fig. 1(a) and (b), for both hexagonal and trigonal space groups respectively [28].

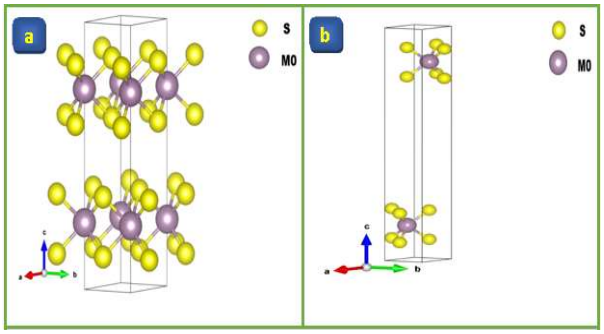

Fig. 1 Structural model of bulk MoS_2 in (a) hexagonal and (b) trigonal phase

The calculated structural properties of the bulk hexagonal and trigonal MoS_2 is presented in Table I and are compared with the available theoretical and experimental results. The bulk MoS_2 has two layers of Mo atoms; one layer is directly above the sulphur atoms of the other layer and vice-versa. After relaxation, the results of the optimized lattice parameters of MoS_2 were compared with recently available calculated values.

Table I. Calculated structural properties of bulk hexagonal and trigonal MoS_2

Bulk MoS_2	*XC*	*a* (Å)	*c* (Å)	*V* (Å^3)	B_0(Gpa)	B'_0	Ref.
Hexagonal	GGA	3.080	13.090	119.41	128.8	4.47	This study
	GGA	3.190	12.310	106.1	50.86	-	[29]
	Exp	3.160	12.290	107.18	47.65	-	[30]
	rvv10	3.218[b]	12.448[b]			-	[31]
Trigonal	GGA	3.45	21.470	194.51	76.6	4.56	This study
	GGA	3.57	18.38	-	-	-	[32]

To investigate the structural stability, the total energy of the two systems was fitted to volume using the Birch-Murnaghan equation of state, shown in (1) with the result of the fit in Table II and plotted in Fig. 2.

Table II. Calculated bulk modulus, volume, pressure derivative, and total energy of MoS_2 using the Murnaghan equation.

```
 equation of state: murnaghan.        chisq =   0.1790D-05
 V0 = 1312.60 a.u.^3,  k0 =  766 kbar,  dk0 =  4.56  d2k0 =  0.000  emin = -993.34764
 V0 =  194.51  Ang^3,  k0 =  76.6 GPa

 ##########################################################################
  Vol.       E_calc       E_fit       E_diff     Pressure      Enthalpy
  a.u.^3       Ry           Ry           Ry         GPa           Ry
 ##########################################################################
 1005.44   -993.03414   -993.03178   -0.00236     39.85      -990.31026
 1034.17   -993.10256   -993.10276    0.00020     33.02      -990.78090
 1063.44   -993.16096   -993.16239    0.00142     27.07      -991.20395
 1093.25   -993.21009   -993.21185    0.00176     21.87      -991.58440
 1123.62   -993.25066   -993.25220    0.00154     17.33      -991.92673
 1154.54   -993.28341   -993.28435    0.00095     13.36      -992.23496
 1186.03   -993.30886   -993.30913    0.00027      9.88      -992.51257
 1218.08   -993.32763   -993.32724   -0.00039      6.82      -992.76273
 1250.70   -993.34028   -993.33932   -0.00096      4.14      -992.98831
 1283.91   -993.34728   -993.34594   -0.00134      1.78      -993.19178
 1317.69   -993.34911   -993.34759   -0.00152     -0.29      -993.37545
 1352.07   -993.34623   -993.34472   -0.00151     -2.12      -993.54136
 1387.03   -993.33899   -993.33771   -0.00129     -3.74      -993.69129
 1422.59   -993.32783   -993.32691   -0.00092     -5.16      -993.82693
 1458.76   -993.31308   -993.31264   -0.00044     -6.42      -993.94974
 1495.53   -993.29501   -993.29516    0.00015     -7.53      -994.06101
 1532.92   -993.27403   -993.27473    0.00071     -8.52      -994.16203
 1570.92   -993.25039   -993.25156    0.00117     -9.40      -994.25386
 1609.55   -993.22430   -993.22584    0.00154    -10.17      -994.33743
 1648.81   -993.19604   -993.19775    0.00172    -10.86      -994.41365
 1688.70   -993.16583   -993.16745    0.00161    -11.48      -994.48333
 1729.22   -993.13387   -993.13506    0.00119    -12.02      -994.54718
 1770.39   -993.10037   -993.10071    0.00035    -12.51      -994.60587
 1812.21   -993.06551   -993.06452   -0.00099    -12.94      -994.66002
 1854.68   -993.02944   -993.02658   -0.00286    -13.33      -994.71012
```

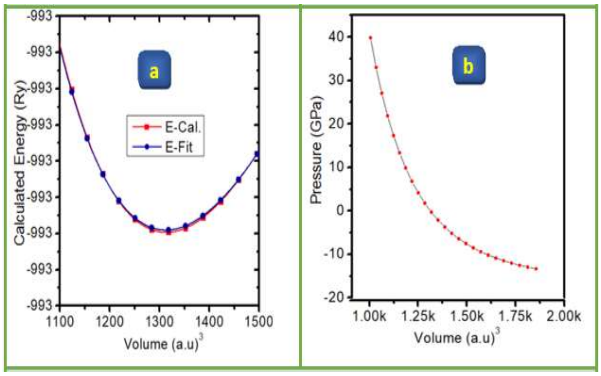

Fig. 2(a) the calculated energy against the volume of trigonal MoS_2 (b) pressure-volume graph of trigonal MoS_2

To determine the reliable theoretical values of the thermodynamical state of the trigonal phase, we use the total energy against the volume which is more reliable than the pressure against the calculated volume as can be seen in Fig. 2(b), by applying the equation of state (EOS) at low cost. The calculated energy-volume fit fully demonstrates the trigonal space group of MoS_2 is thermodynamically stable as can be seen in Fig. 1(a).

$$E(V) = E_0 + \frac{9V_0B_0}{16}\left[\left\{\left(\frac{V_0}{V}\right)^{\frac{2}{3}} - 1\right\}^2 B_0' + \left\{\left(\frac{V_0}{V}\right)^{\frac{2}{3}} - 1\right\}^2 \left\{\left\{6 - 4\left(\frac{V_0}{V}\right)^{\frac{2}{3}}\right\}\right\}\right] \quad (1)$$

Where E_0 is the ground state energy, V_0 is the equilibrium volume and v is the deformed volume, B_0 is the bulk modulus, and B_0' is the derivative of the bulk modulus.

B. Electronic band structure and density of states

To demonstrate the nature and the orbital contribution of the total density of state (TDOS) of the electronic energy band gaps of the two space groups MoS_2, the knowledge of the total density of state and partial density of the state is critical. In this regard, the calculated bandgaps for the two phases of the material have been recorded alongside the experimental results in Table III.

Table III. Calculated energy bandgap of hexagonal and trigonal bulk of MoS_2

Bulk MoS_2	XC	bandgap (eV)	Ref.
Hexagonal	GGA	1.37	This study
		1.23	[33]
		1.29	[34]
	rvv10	0.85	[35]
		0.89	[36]
Trigonal	GGA	1.56	This study

The electronic band structure and corresponding density of states or the hexagonal and trigonal bulk phases of MoS_2 are shown in Fig. 3(a) and Fig. 4(a) respectively using GGA exchange-correlation, following the high symmetry points $\Gamma - M - K - \Gamma$, in the first Brillion zone, the partial and total density of state of hexagonal and trigonal were also shown in Fig. 3(b) and 4(b) respectively. The electronic band structure and density of states of the bulk hexagonal MoS_2 are divided into three energy states from the valence to the conduction bands spanning from -7.0 to $+7.0$ eV states respectively. For the hexagonal structure, the first group of bands in the electronic band structure and density of states around -7.00 to -1.00 eV is mainly due to the 3p and 4d states of S and Mo atoms [32]. The second group is Fermi energy in the energy range from -1.0 to 0.6 eV with no state contributing. In the third group above the Fermi energy, the energy range is 0.6 to 7.0 eV, the main contribution is due to 4d orbitals of Mo, and 3p of the S atom which is the main contribution, and it shows a strong hybridization. Similarly, the trigonal electronic band structure and density of states around -7.00 to -1.00 eV in the valence band are mainly due to the 3p and 4d state of S and Mo atoms contributing to the peaks in the TDOS [33]. The second group in the energy range from -1.00 to 0.75 eV within the Fermi energy state holds the calculated bandgaps of the trigonal bulk MoS_2 materials. In the third group above the Fermi energy, the energy range is between 0.75 eV and above in the conduction bands are mainly contributions from the 4d state of Mo and 3p energy state of S. The PDOS analysis demonstrates high contribution by 4d and 3p states of Mo and S respectively.

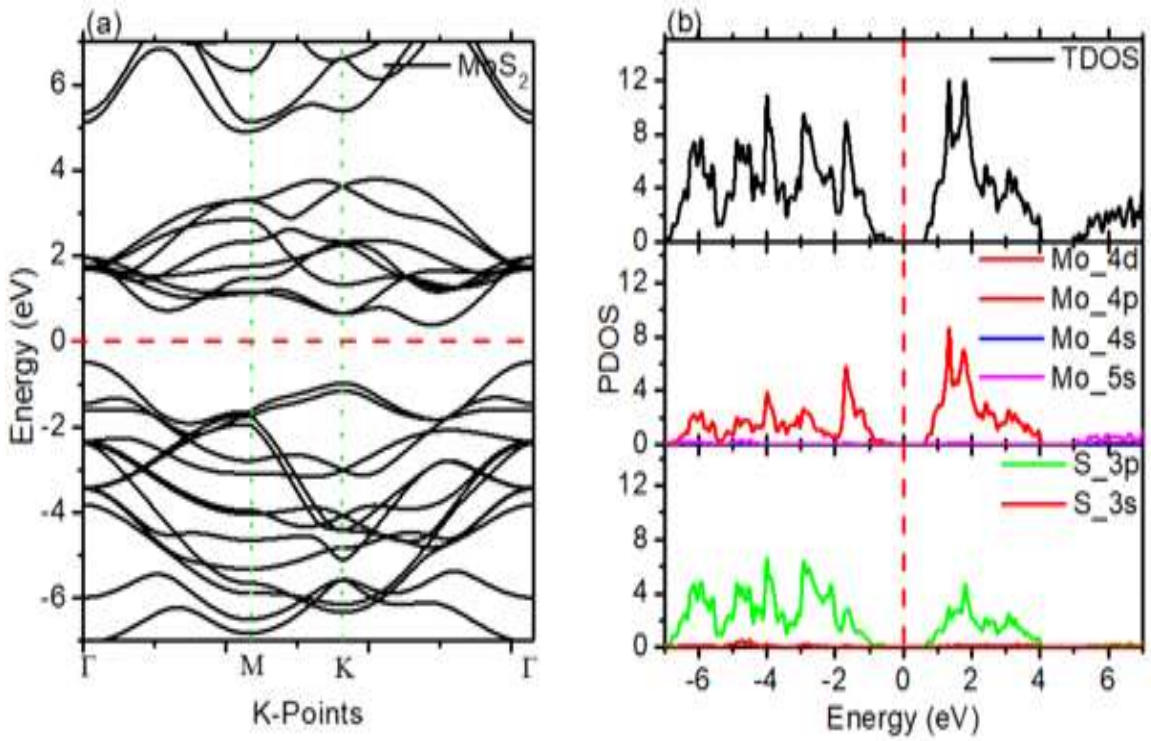

Fig. 1 Calculated (a) electronic energy bandgap and (b) density of states of hexagonal MoS_2 using GGA

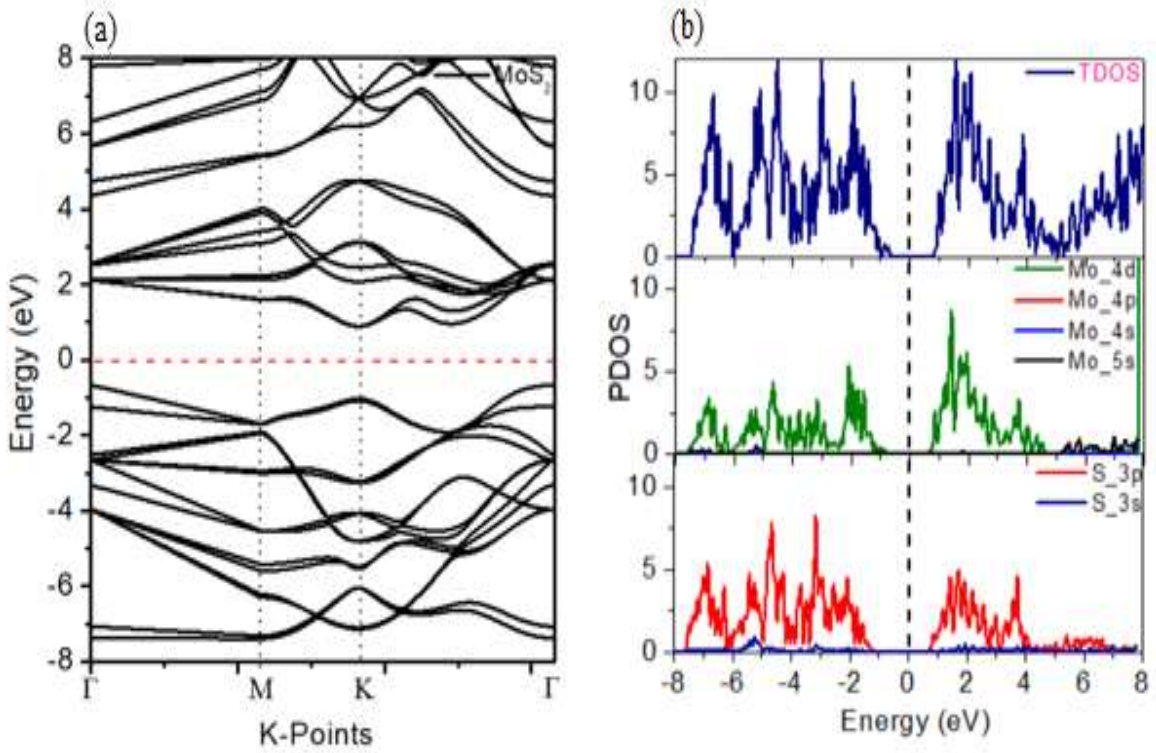

Fig. 2 Calculated (a) electronic energy bandgap and (b) density of states of trigonal MoS_2 using GGA-PBE

To further demonstrate the electronic band gap, the bands around the forbidden gap are relatively flat, as expected from the '*d*' orbital. For bulk hexagonal MoS_2, the valence band maximum is at Γ and the conduction band minimum is in between K and Γ direction of the hexagonal phase of MoS_2 revealing an indirect band-gap semiconductor, as can be seen in Fig. 3(a). For trigonal bulk MoS_2, the valence band maximum is also at Γ and the conduction band minimum is at K high symmetry point revealing an indirect bandgap semiconductor as can also be seen in Fig. 4(a). Although our calculated band gaps for bulk MoS_2 are in good agreement with theoretical values obtained in [33], they underestimate the experimental band gap due to the inherent drawback of standard GGA functionals. Our calculated values of the band gap for hexagonal bulk MoS_2 using GGA are $1.37\ eV$ and $1.52\ eV$ for trigonal bulk MoS_2, which is in very good agreement with the results obtained in [12, 31-33]. In addition, it is found that the TDOS of hexagonal and trigonal phases are slightly similar as can be seen in Fig. 2(b) and 3(b), this is because both the two phases of MoS2 are mainly composed with Mo_4d, S_3p, and S_3s state to the TDOS. The added conduction band of hexagonal MoS_2 migrates from the high-energy region to the Fermi level, as a result, it promotes the electron transfer between the valence and the conduction band. This gives us a clear understanding of why the band gap of the hexagonal phase is smaller than the trigonal phase.

C. Mechanical properties

Several significant solid-state properties of crystals are connected to elastic properties, such as the equation of states, Debye temperature, mechanical properties, etc. Elastic modulus and elastic constants can provide a complete understanding of the structural behaviors of materials such as the stability of a material, hardness, ductility, brittleness, and other mechanical properties. In this Section, we focused on the crystal stability of the two space groups of MoS_2. To study and compute the elastic constants of these systems, the system responses to the applied stress need to be studied and analyzed from which all the elastic constants can be determined. In this work, we used Thermo-pw, auxiliary software in Quantum ESPRESSO code to calculate the responses of MoS_2 to applied stress. Molybdenum disulfide exists in hexagonal and trigonal space groups and both have five independent elastic constants C_{11}, C_{12}, C_{13}, C_{33}, and C_{44}, there exists in the calculations C_{66} [34] which is dependent on these five elastic constants, given by $C_{66} = (C_{11} - C_{12}) / 2$. Our calculated elastic constants for both hexagonal and trigonal are presented in Table 3 alongside available theoretical and experimental results [35]. The results obtained from the hexagonal space group are in total agreement with the experimental results in [36]. C_{12} and C_{13} are moderately close to the theoretical result obtained by [17]. To the best of our knowledge, there is no available result to compare with the trigonal space group MoS_2. Under isotropic pressure, the mechanical stability of the two phases of both hexagonal and trigonal systems obeys the Born mechanical stability criteria [37], as given by (1) to (3). The calculated elastic constants shown in (4) satisfy the Born stability criteria, suggesting that both phases of MoS_2 are mechanically stable at zero pressure.

$$C_{11} > 0, C_{33} > 0, C_{44} > 0 \quad (1)$$

$$(C_{11} - C_{12}) > 0 \quad (2)$$

$$(C_{11} + C_{12}) > C_{33} - 2C_{13}^2 > 0 \quad (3)$$

Table IV shows that both hexagonal and trigonal elastic constants are positive, indicating that the two compounds are stable. The ratios C_{33}/C_{11} and C_{13}/C_{12} show that atomic bonding along the x-direction is stronger than that along the z-direction for both hexagonal and trigonal atoms as can be seen in (3). Currently, to the best of our knowledge, there is no experimental or theoretical data on the trigonal space group for comparison.

Table IV. Calculated elastic constants at zero pressure using GGA-PBE for bulk hexagonal and trigonal MoS_2

Phase	XC	C_{11}	C_{12}	C_{13}	C_{33}	C_{44}	C_{33}/C_{11}	C_{13}/C_{12}	Ref
Hexagonal		191	46	-5	15	7	0.08	-0.11	This study
		211	49	3	37	30	-	-	[17]
		238	64	12	57	18	-	-	[35]
	EXP	238	-54	23	52	19	-	-	[36]
Trigonal		124	29	-3	7	2	0.07	-0.10	This study

D. Elastic modulus and hardness

The bulk modulus B together with the C_{44} can assess the machinability of the compounds via the machinability index $\mu = B/C_{44}$, μ provides the value that determines the degree to which a particular compound will be cut into different shapes. The higher value of μ the better the machinability. In this work, we have estimated the bulk modulus (B), the shear modulus (G), and the young modulus (Y) for the individual C_{ij} for both hexagonal and trigonal structures respectively to determine their effect on the physical properties of the materials. Table V shows the calculated mechanical properties of the two structures. While the bulk modulus (B) describes the average atomic bond strength, the shear modulus (G) measures the resistance to restrict deformation upon shear stress. This demonstrates that there is a direct relationship between bulk modulus and shear modulus, implying that in the hunt for the hardness of a material, a large bulk modulus or shear modulus is required. The Pugh rule is used to estimate whether the MoS_2 will be brittle or ductile (B/G = 1.75) [39]. The proposed B/G ratio for determining material ductility and brittleness is around 1.75. If the B/G ratio is more than 1.75, the material is ductile; otherwise, it is brittle. In this work, the computed B/G values for hexagonal and trigonal space groups are 1.35 and 1.40, respectively, suggesting that both space groups are brittle at 0 GPa. To further demonstrate the nature of the bonding properties, we employ the service of the poison ratio, which tells information about the bonding of the system. For covalence, the poison ratio is usually less than 0.25 for all materials. Our findings in Table 4 show that the poison ratio

of the hexagonal and trigonal phases of MoS_2 is 0.20 and 0.21 respectively. However, our results clearly show that both space groups of MoS_2 have covalent properties. Therefore, the covalent contribution for inter-atomic bonding is predicted for the two space groups of MoS_2.

Table V. The calculated bulk moduli *B* in GPa, shear moduli *G* in GPa, Young modulus *E* in GPa, Pugh's ratio *G/B*, and Poisson's ratio at zero pressure.

Phase	*B*	*G*	*Y*	*B/G*	*v*	*μ=B/C44*	θ_D	Ref
hexagonal	35	26	63	1.35	0.20	5.00	211.270	This study
Hexagonal	51	47	107	1.09			278.35	[17]
Exp	53							
Trigonal	21	15	36	1.40	0.21	10.50	143.025	This study

For the hexagonal or trigonal space group crystal structure of MoS_2, the bulk, and the shear modulus are represented by (4) to (7). Equations (9) and (10) represent Young modulus (E) and Poisson's ratio (υ).

Reuss's approximation is given by (5) and (6) and Hill's approximation is also given by (7) and (8).

$$G_R = \frac{[(C_{11}+C_{13})C_{33}-2C_{13}^2]}{2[3B_vC_{44}C_{66}+\{(C_{11}+C_{12})C_{33}+2C_{13}^2\}(C_{44}+C_{44})]} \quad (5)$$

$$B_R = \frac{(C_{11}+C_{13})C_{33}-2C_{13}^2}{C_{11}+C_{12}+2C_{33}+4C_{13}} \quad (6)$$

$$G_v = \frac{1}{30}(+C_{11}+C_{12}-2C_{33}+4C_{13}+12C_{44}+12C_{66}) \quad (7)$$

$$B_v = \frac{1}{2}[2(C_{11}+C_{12})+4C_{13}-C_{33}] \quad (8)$$

Young modulus E and Poisson's ratio can be deduced from the following relation:

$$E = \frac{9BG}{3B+G} \quad (9)$$

$$\upsilon = \frac{3B-2G}{2(3B+G)} \quad (10)$$

The actual effective modulus of anisotropic polycrystalline crystals from the arithmetic means of these two values as approximated by Hill [40] the shear modulus and the bulk modulus are defined as:

$$G = \frac{1}{2}(G_R+G_v) \quad (11)$$

$$B = \frac{1}{2}(B_R+B_v) \quad (12)$$

The Young modulus of a material is defined as the ratio of longitudinal stress and longitudinal strain, which is used to measure the stiffness of the solid material. A higher value of Young modulus indicates the stiffness of the material. From Table V, the hexagonal space group is stiffer than the trigonal space group. Another critical parameter that relates many physical properties of solids, such as their specific heat and melting temperatures is known as Debye temperature. The Debye temperature is obtained from the calculated elastic constants, which can be computed using (13).

$$\Theta_D = \pi r^2 = \frac{\hbar}{\varkappa}\left[\frac{3n}{4\pi}\left(\frac{N_A\rho}{M}\right)\right]^{\frac{1}{3}}V_m \quad (13)$$

$\hbar$ is Planck's constant.

$$V_m = \left[\frac{1}{3}\left(\frac{2}{V_S^3+V_l^3}\right)\right]^{\frac{-1}{3}} \quad (14)$$

$$V_s = \sqrt{\frac{G}{\rho}}.K(v) \quad (15)$$

$$V_l = \sqrt{\frac{B+(4/3)G}{\rho}} \quad (16)$$

Where N_A, is Avogadro's number, ρ is the density M, the molecular weight, V_m the average sound velocity, V_l the longitudinal sound velocity and V_t the transverse sound velocity.

E. Anisotropy

The orientation dependency of the elastic moduli or sound velocities is known as crystal elastic anisotropy [40]. The anisotropy can be defined by the three elastic independent shear constants. The hexagonal and trigonal shear anisotropy factors are given by (17) to (18) and the value of $^{K_c}/_{K_a}$ is also computed. Table VI presents all the calculated anisotropy factors from independent elastic constants of hexagonal and trigonal phases [41].

$$A_1 = \frac{^1/_6(C_{11}+C_{12}+2C_{33}-4C_{13})}{C_{44}} \quad (17)$$

$$A_2 = \frac{2C_{44}}{C_{11}-C_{12}} \quad (18)$$

$$A_3 = \frac{^1/_3(C_{11}+C_{12}+2C_{33}-4C_{13})}{C_{11}-C_{12}} \quad (19)$$

Table VI. Anisotropy factors for bulk hexagonal and trigonal MoS_2.

Phase	A_1	A_2	A_3	K_c/K_a	Ref
Hexagonal	6.89	0.09	0.66	11.35	This study
Trigonal	9.94	0.04	0.34	10.70	This study

Table VI shows the hexagonal and trigonal phases of MoS_2 and the shear anisotropic factors calculated. A system with Anisotropy equal to 1 shows an isotropic property, while any value smaller or larger than 1 implies the material is anisotropic. The magnitude of the deviation from 1 is a measure of the degree of elastic anisotropy possessed by a crystal. Any value of $^{K_c}/_{K_a}$ less than 1 reveals the compressibility along the c-axis is smaller than that along the a-axis otherwise the compressibility along the c-axis is larger than that along the a-axis. Our calculated values for $^{K_c}/_{K_a}$ for both hexagonal and trigonal phases at zero pressure are 10.35 and 10.07 respectively, the calculated directional bulk modulus of the two space groups suggest that their value are larger along the a-axis than on the c-axis, which indicate that the compressibility along the a-axis is smaller.

IV. CONCLUSION

The first-principle DFT calculation was used to calculate the structural, electronic, and elastic properties of bulk MoS_2 in hexagonal and trigonal phases as implemented in the Quantum ESPRESSO simulation code. Results obtained revealed that the hexagonal phase of MoS_2 is much more stable than the trigonal space group. This study shows that

both space groups are semiconductors with an indirect bandgap of 1.37 and 1.56 eV for Hexagonal and trigonal phases respectively. The elastic properties demonstrated that both space groups satisfy Born's mechanical stability condition. The higher value of the Young modulus observed in the hexagonal phase indicates that the phase is stronger than the trigonal phase. Finally, the overall results place the new optimized MoS_2 as a potential candidate for the next generation of sustainability science and technology to pave way for many technological applications.

ACKNOWLEDGMENT

The authors of this study acknowledge the Universiti of Teknologi Malaysia for providing computational condensed matter training to the lead researcher.

Reference

[1] D. Junli, H. Yu, B. Liu, M. Hong, Q. Liao, Z. Zhang and Y. Zhang, "Strain engineering in 2D material-based flexible optoelectronics". *Small Methods, vol.* 5, no. 1, pp. 2000919, 2021.

[2] Y. See-Hun, R. Naaman, Y. Paltiel and S. S. P. Parkin, "Chiral spintronics". Nat. Rev. Phy. vol. 3, no. 5, pp. 328-343, 2021.

[3] K. Han-gyu and H. J. Choi, "Quasiparticle band structures of bulk and few-layer PdSe 2 from first-principles G W calculations". Phy. Rev. B, vol. 103, no. 16, pp. 165419, 2021.

[4] S. Jie, X. Li, W. Guo, M. Zhao, X. Fan, Y. Dong, C. Xu, J. Deng and Y. Fu, "Synthesis methods of two-dimensional MoS_2: A brief review". Crys. vol. 7, no. 7, pp. 198, 2017.

[5] P. G. Dimitrios, I. A. Kinloch and R. J. Young, "Mechanical properties of graphene and graphene based nano composites".Prog.in Mat. Sci., vol. 90, pp. 75-127, 2017.

[6] Y. S. Aminu, A. Shaari, and I. Isah, "Structural stability, Electronic and Optical Properties of Bulk MoS_2 Transition Metal Dichalcogenides: A DFT Approach". J. Appl. Phy., vol. 14, pp. 40, 2022.

[7] N. A. H Castro, F. Guinea, N. M. R. Peres, K. S. Novoselov and A. K. Geim, "The electronic properties of graphene". Rev. of Modern Phy. vol. 81, no. 1, pp. 109, 2009.

[8] P. Puspamitra, T. Hussain, A. Karton and R. Ahuja, "Elemental substitution of two-dimensional transition metal dichalcogenides ($MoSe_2$ and $MoTe_2$): implications for enhanced gas sensing". ACS Sens., vol. 4, no. 10, pp. 2646-2653, 2019.

[9] C. Wonbong, I. Lahiri, R. Seelaboyina and Y. S. Kang, "Synthesis of graphene and its applications: a review". Crit. Rev. in Sol. St. & Mat. Sci. 35, no. 1, pp. 52-71, 2010.

[10] U. M. Miguel, A. J. Bradley, S. Shi, F. H. D. Jornada, Y. Zhang, D. Y. Qiu, W. Ruan, et al., "Giant bandgap renormalization and excitonic effects in a monolayer transition metal dichalcogenide semiconductor". Nat. Mat., vol. 13, no. 12, pp. 1091-1095, 2014.

[11] C. Shuang, Y. Pan, D. Wang and H. Deng, "Structural Stability and Electronic and Optical Properties of Bulk WS 2 from First-Principles Investigations" J. of Elect. Mat., vol. 49, pp. 7363-7369, 2020.

[12] H. N. Nguyen, V. V. Ilyasov, T. V. Vu, N. A. Poklonski, H. V. Phuc, L. T. T. Phuong, B. D. Hoi, and C. V. Nguyen, "First-principles study of optical properties of molybdenum disulfide: From bulk to monolayer". Superlatt. & Microstruct., vol. 115, pp. 10-18, 2018.

[13] S. Ahmad and S. Mukherjee, "A Comparative Study of Electronic Properties of Bulk MoS_2 and its Monolayer using DFT Technique: Application of Mechanical Strain on MoS_2 Monolayer. Graphene, vol. 3, pp. 52-59, 2014.

[14] T. Böker, R. Severin, A. Müller, C. Janowitz, R. Manzke, D. Voß, P. Krüger, A. Mazur and J. J. P. R. B. Pollmann, "Band structure of MoS_2, $MoSe_2$, and α− $MoTe_2$: Angle-resolved photoelectron spectroscopy and ab initio calculations". Phy. Rev. B, vol. 64, no. 23, pp. 235305, 2001.

[15] Mak, Kin Fai, Changgu Lee, James Hone, Jie Shan, and Tony F. Heinz. "Atomically thin MoS_2: a new direct-gap semiconductor." Phy. Rev. Lett., vol. 105, no. 13 (2010): 136805.

[16] F. Lahourpour, et al., "Structural, electronic and optical properties of graphene-like nano-layers MoX_2(X: S, Se, Te): DFT study". J. of Theo. & App. Phy., vol. 13, no. 3, pp. 191-201, 2019.

[17] L. Wei, et al., "Electronic and elastic properties of MoS_2". Phy. B: Cond. Mat., vol. 405, no. 10, pp. 2498-2502, 2010.

[18] J. N. Yuan, et al., "First-principles study of electronic and elastic properties of hexagonal layered crystal MoS_2 under pressure". Zeitschrift für Naturforschung A, vol. 70, no. 7, pp. 529-537, 2015.

[19] S. Sarma and S.C. Ray, "Trigonal (1T) and hexagonal (2H) mixed phases MoS_2 thin films". App. Surf. Sci., vol. 474, pp. 227-231, 2019.

[20] Z. Zeng, et al., "Single-layer semiconducting nanosheets: high-yield preparation and device fabrication". Angewandte Chemie, vol. 123, no. 47, pp. 11289-11293, 2011.

[21] M. de Jong, et al., "The high-throughput highway to computational materials design". Sci. Data, vol. 2, pp. 150009, 2013.

[22] D. Bagayoko, "Understanding density functional theory (DFT) and completing it in practice". AIP Adv., vol. 4, no. 12, pp. 127104, 2014.

[23] P. Dufek, P. Blaha and K. Schwarz, "Applications of Engel and Vosko's generalized gradient approximation in solids. Phy. Rev. B, vol. 50, no. 11, pp. 7279, 1994.

[24] P. Giannozzi, et al., "Advanced capabilities for materials modeling with Quantum ESPRESSO. J. of Phy: Cond. Mat., vol. 29, no. 46, pp. 465901, 2017.

[25] P. Giannozzi, et al., "Quantum ESPRESSO toward the exascale". The J. of Chem. Phy., vol. 152, no. 15, pp. 154105, 2020.

[26] H. J. Monkhorst and J.D. Pack, "Special points for Brillouin-zone integrations. Phy.l Rev. B, vol. 13, no. 12, pp. 5188, 1976.

[27] A. S. Rosen, et al., "Machine learning the quantum-chemical properties of metal-organic frameworks for accelerated materials discovery". Mat., vol. 4, no. 5, pp. 1578-1597, 2021.

[28] J. A. Wilson and A. D. Yoffe, "The transition metal dichalcogenides discussion and interpretation of the observed optical, electrical and structural properties". Adv. in Phy. vol. 18, no. 73, pp. 193-335, 1969.

[29] C. Ataca, et al., "Mechanical and electronic properties of MoS_2 nanoribbons and their defects". The J. of Phy. Chem. C, 115(10): p. 3934-3941, vol. 115, no. 10, pp. 3934-3941, 2011.

[30] H. Peelaers and C. Van de Walle, "Elastic constants and pressure-induced effects in MoS_2". The J. of Phy. Chem. C, vol. 118, no. 22, pp. 12073-12076, 2014.

[31] J. L. Feldman, "Elastic constants of 2H-MoS_2 and 2H-$NbSe_2$ extracted from measured dispersion curves and linear compressibilities". J. of Phy. & Chem. of Sol., vol. 37, no. 12, pp. 1141-1144, 1976.

[32] M. Born, "On the stability of crystal lattices". In Math. Proceed, of the Cambridge Phy. Soc. Cambridge University Press, 1940.

[33] Y. S. Aminu, A. Shaari, N. A. M Alsaif, I. M. Alsalamah, I. Isah, and N. Rekik, "Elucidating the Structural, Electronic, Elastic, and Optical Properties of Bulk and Monolayer MoS_2 Transition-Metal Dichalcogenides: A DFT Approach." ACS omega, vol. 7, no. 49, pp. 45719-45731, 2022.

[34] W. Zifeng, Z. Huang, N. Lu, J. Guan and Y Hu, "An energy transfer and patterning characteristics in pulsed-laser subtractive manufacturing of single layer of MoS_2." International Journal of Heat and Mass Transfer vol. 204, pp. 123873, 2023.

[35] Y. Nassah, A. Benmakhlouf, L. Hadjeris, T. Helaimia, R. Khenata, A. Bouhemadou, S. Bin Omran, R. Sharma, S. G. Said and V. Srivastava, "Electronic band structure, mechanical and optical characteristics of new lead-free halide perovskites for solar cell applications based on DFT computation". Bulletin of Mat. Sci., vol. 46, no. 2, pp. 55, 2023.

[36] Y. Pan and D. Pu, "Hydrogen embrittlement of C40 transition-metal disilicides. Journal of Materials Research, vol. 34, 18, pp. 3163-3172, 2019.

[37] R. Hill, "The elastic behavior of a crystalline aggregate. Proceed. of the Phy. Soc. Sect. A, vol. 65, no. 5, pp. 349, 1952.

[38] S. Assouline and D. Or, "Anisotropy factor of saturated and unsaturated soils". Wat. Resources. Res., vol. 42, 12, 2006.

[39] Y. Nassah, A. Benmakhlouf, L. Hadjeris, T. Helaimia, R. Khenata, A. Bouhemadou, S. Bin Omran, R. Sharma, Souraya Goumri Said and V. Srivastava, "Electronic band structure, mechanical and optical characteristics of new lead-free halide perovskites for solar cell applications based on DFT computation", Bulletin of Mat. Sci., vol. 46, no. 2, pp. 55, 2023.

[40] P. N. Guillermo, L. A. Lozano, R. Villarreal, M. P. Salazar, E. M. Melani and C. G. Soracco, "Cover crops effects on anisotropy of unsaturated soil hydraulic properties". Soil and Tillage Res., vol. 227, 105601, 2023.

[41] Y. S. Aminu, A. Shaari and I. Isah, "Structural stability, Electronic and Optical Properties of Bulk MoS_2 Transition Metal Dichalcogenides: A DFT Approach". J. Appl. Phy, vol. 14, pp. 40, 2022.